The Cryosphere Discuss., 7, 5255–5279, 2013
www.the-cryosphere-discuss.net/7/5255/2013/
doi:10.5194/tcd-7-5255-2013

The Cryosphere Discussions
Open Access

Measuring the specific surface area of wet snow using 1310 nm reflectance

J.-C. Gallet[1], F. Domine[2,3], and M. Dumont[4]

[1]Norwegian Polar Institute, Tromsø, Norway
[2]Takuvik Joint International Laboratory, Université Laval (Canada) and CNRS-INSU (France), Pavillon Alexandre Vachon, 1045 avenue de La Médecine, Québec, QC, G1V 0A6, Canada
[3]Department of Chemistry, Université Laval, Québec, QC, Canada
[4]Météo-France – CNRS, CNRM-GAME UMR3589, CEN, Grenoble, France

Received: 1 October 2013 – Accepted: 16 October 2013 – Published: 31 October 2013

Correspondence to: F. Domine (florent.domine@gmail.com)

Published by Copernicus Publications on behalf of the European Geosciences Union.

Abstract

The specific surface area (SSA) of snow can be used as an objective measurement of grain size and is therefore a central variable to describe snow physical properties such as albedo. Snow SSA can now be easily measured in the field using optical methods based on infrared reflectance. However, existing optical methods have only been validated for dry snow. Here we test the possibility to use the DUFISSS instrument, based on the measurement of the 1310 nm reflectance of snow with an integrating sphere, to measure the SSA of wet snow. We perform cold room experiments where we measure the SSA of a wet snow sample, freeze it and measure it again, to quantify the difference in reflectance between frozen and wet snow. We study snow samples in the SSA range 12–37 $m^2\,kg^{-1}$ and in the mass liquid water content range 5–32 %. We conclude that the SSA of wet snow can be obtained from the measurement of its 1310 nm reflectance using three simple steps. In most cases, the SSA thus obtained is less than 10 % different from the value that would have been obtained if the sample had been considered dry, so that the three simple steps constitute a minor correction. We also run two optical models to interpret the results, but no model reproduces correctly the water-ice distribution in wet snow, so that their predictions of wet snow reflectance are imperfect.

1 Introduction

Snow is a porous medium made of air, ice, small amounts of impurities and occasionally liquid water. It is the most reflective surface on Earth so that its albedo is a key parameter to determine the planetary energy budget (Hall, 2004; Lemke et al., 2007). The albedo of snow is determined mostly by its impurity content and grain size but the liquid water content also plays a role (Warren, 1982). In the visible range of the solar spectrum, the albedo of dry snow is little dependent on the snow grain size and is mostly controlled by the impurity content. In the infra-red, snow grain size controls the

TCD
7, 5255–5279, 2013

albedo of dry snow (Warren, 1982). The effect of water on snow albedo depends on its location. When present in small amounts, water is located only at grain boundaries (Colbeck, 1973) and a slight decrease in albedo is observed (Wiscombe and Warren, 1980). For a high water fraction, water entirely coats the snow grains so that large water-ice clusters are formed resulting in a larger decrease in albedo (Colbeck, 1973).

Even if the contrast between water and ice refractive index is small, maxima and minima for water are shifted towards shorter wavelengths, as shown in Fig. 1 (Segelstein, 1981; Warren and Brandt, 2008) so that a spectral signature is expected when sufficient amounts of water are present in the snowpack (Green et al., 2002), in particular in the 950–1150 nm range. Several investigations of the spectral signature of snow surfaces have been carried out in the past in that range of wavelengths for remote sensing purposes, in order to retrieve the snow grain size and/or liquid water content (Dozier and Painter, 2004; Green et al., 2002, 2006; Nolin and Dozier, 2000). Nolin and Dozier (2000) concluded that the effect of liquid water is negligible in the 950–1150 nm range for the purpose of snow grain size retrieval if the amount of water is lower than 5 % per mass. In that wavelength range, the spectral shift between ice and water is at its maximum. At 1310 nm, ice and water present close values of indices of refraction (1.5 and 26 % higher for water respectively for the real and the imaginary parts) so that the effect of water should be weak as well. The present work describes the possibility of retrieving grain size of wet snow from the measurement of reflectance at 1310 nm.

Given the highly variable shapes of snow grains, the notion of "snow grain size" has long been not very well defined and varies from one study to another (Aoki et al., 2000). More recent studies have used the surface/volume ratio, i.e. the snow Specific Surface Area (SSA) to determine the optical properties of the snow. The snow SSA is defined as the surface area per unit mass (Legagneux et al., 2002),

$$\mathrm{SSA} = \frac{S}{M} = \frac{S}{\rho_{\mathrm{ice}} \times V} = \frac{3}{\rho_{\mathrm{ice}} \times r_{\mathrm{eff}}} \quad (1)$$

with S the surface area of snow grains, M their mass, V their volume, ρ_{ice} the density of ice (917 kg m^{-3} at 0 °C) and r_{eff} the effective radius of the snow grains, i.e. the radius

TCD
7, 5255–5279, 2013

of ice spheres having the same SSA as the snow. This radius is sometimes called the optical radius. For dry snow, the SSA quantifies the ice/air interface per unit mass. For wet snow, it quantifies the sum of the ice/air and water/air interfaces per unit mass. The snow SSA is a physical quantity that requires no assumption regarding grain shape and is expressed in $m^2\,kg^{-1}$ with measured values ranging from 7 to 223 $m^2\,kg^{-1}$ for dry snow (Domine et al., 2007, 2011).

In field studies, when wet snow is encountered, air temperature is often above 0 °C so that the sample cannot be refrozen on site. All current snow SSA measurements techniques have been developed and validated for dry snow. Many techniques, such as CH_4 adsorption (Domine et al., 2007) or X-ray tomography (Flin et al., 2004), cannot be used because they require that the snow be frozen. Optical methods, on the other hand, are potentially appropriate. Such methods have been used to measure the SSA of dry snow (Arnaud et al., 2011; Gallet et al., 2009; Matzl and Schneebeli, 2006; Montpetit et al., 2012; Painter et al., 2007; Picard et al., 2009) but none has been tested for wet snow. Here we used the DUFISSS instrument (Gallet et al., 2009) to measure the 1310 nm reflectance of wet snow. Briefly, Gallet et al. (2009) used an integrating sphere to measure the reflectance of a snow sample at 1310 or 1550 nm and determined its SSA with a calibration curve obtained by the simultaneous measurement of reflectance and SSA using CH_4 adsorption. The shorter wavelength was used for SSA lower than 60 $m^2\,kg^{-1}$ while the longer one was used for higher snow SSA. The estimated accuracy of this instrument is 10 % and allows a fast measure of SSA in the field for every type of dry snow.

To extend the validation of the method to wet snow, experiments were performed in a cold room. We used DUFISSS to measure the 1310 nm reflectance of wet snow of known density and liquid water content (LWC). We then let the wet snow sample refreeze and measured its reflectance again, so that the reflectances of the same snow sample, wet and frozen, can be compared. Radiative transfer calculations using the DISORT model (Stamnes et al., 1988) are also used in order to compare our cold room data set with theoretical calculations.

TCD
7, 5255–5279, 2013

2 Experimental protocol

The idea of our cold room experiments was to prepare a homogeneous wet snow sample. We then measured its density and LWC and took a sample whose reflectance was measured at 1310 nm with DUFISSS placed in a cold room at −2.2 °C. The sample was then allowed to refreeze without any disturbance to its structure so that the reflectance of the very same sample could be measured again once refrozen. The hypothesis here is that freezing does not lead to any detectable change in structure, apart from the volume expansion. Since SSA is the surface area to mass ratio, freezing, which expands volume and therefore surface area, increases SSA.

The snow used was taken from large plastic boxes filled with snow from the nearby mountains and stored at −20 °C. Snow from two distinct snowfalls was used, one about a week old and the other from the previous season. To make uniform samples, batches of about 500 g of snow were mixed in a dough kneader placed in a cold room at −2.2 °C. Several such batches were placed inside a large plastic box and were further mixed with a shovel. The resulting sample was then transferred into a plexiglas box 15 cm × 25 cm in horizontal section and 25 cm in height.

To obtain a wet snow sample, we used the method detailed by (Brun et al., 1988). Briefly, the plexiglas box was placed between 2 conductor plates within an insulated box, and between these plates a current of 4000 V at 20 kHz was applied. The instrument was also located in the cold room at −2.2 °C. At 20 kHz frequency, the energy absorption by snow is such that homogeneous heating is produced, so that a uniform LWC content can be obtained. Of course, the LWC is not perfectly uniform because of conductive losses at the edges. Furthermore, at high LWC, percolation can take place. However, for our purpose, possible moderate variations in LWC within the box are not critical.

Six snow samples were heated for durations between 23 and 90 min. The plexiglas box was then taken out of the heater and placed on a bench in the cold room at −2.2 °C. Snow density was then measured using a 100 cm^3 tubular cutter which was weighted,

TCD
7, 5255–5279, 2013

showing densities between 153 and 296 kg m^{-3}. The LWC was determined using the apparatus described in (Brun et al., 1988). Briefly, the relative permittivity of the snow was measured in a cylindrical capacitor of 330 cm^3 at a frequency around 18 MHz. LWCs between 5 and 32 % in mass were obtained.

Two snow samples were then taken for IR reflectance measurements at 1310 nm using the exact protocol detailed in Gallet et al. (2009). Briefly, a cylindrical snow core 63 mm in diameter and 30 mm high was placed in a 25 mm high cylindrical container. The extra 5 mm were then shaved off with a metal spatula. Ideally, the spatula should be exactly at 0 °C so that no freezing or melting occurs. Initially the spatula was at −2.2 °C in the cold room. After trial and error, holding the spatula between both gloved hands for 3 s appeared to minimize disturbance to the sample structure, in that neither glazing from a too cold spatula nor no appearance of extra liquid water was observed. In any case, the penetration depth of the 1310 nm radiation in the snow types studied was about 1 cm (Gallet et al., 2009), so that minimal surface perturbation due to our careful protocol most likely had little influence on measured reflectance. The snow sample was then allowed to freeze. A total of 12 samples were thus measured, two for each experiment. Since density, LWC and reflectance required distinct samples, and since given the amount of snow available only one density and one LWC measurement were done, the density and LWC values found were ascribed to both snow samples whose reflectance were measured, even though there were certainly slight variations within the plexiglas box. The SSA was computed from reflectance using a polynomial fit of the SSA-reflectance relationship as described in Gallet et al. (2009). Here, we use the same relationship for wet and dry snow, although it only holds for dry snow and the value obtained for wet snow is therefore only an apparent SSA (SSA_{app} hereafter), from which we subsequently try to extract the actual wet snow SSA.

TCD
7, 5255–5279, 2013

3 Models description

The modeling study is the same as that used by (Green et al., 2002). It is based on the Discrete-ORdinate Radiative Transfer code (DISORT) (Stamnes et al., 1988). DISORT calculates the reflectance of a succession of horizontally infinite plane-parallel snow layers under direct and/or diffuse illumination knowing the optical properties of each layer. The required input properties, namely the single scattering albedo, the extinction efficiency and the phase function are calculated using either of the following two codes: Mie (Wiscombe and Warren, 1980) or the layered-sphere Mie calculations (Toon and Ackerman, 1981). The differences between both models is therefore only due to the use of either Mie or the layered code.

Mie calculations were used for spherical ice grains and liquid water spheres. This results in droplets of water being present in the interstitial space between ice grains. Optical properties were calculated for both materials and mixed by weighted average (Warren and Wiscombe, 1980). The second approach is the layered calculation which represents snow as spheres made of a core of ice and a shell of water. In both cases, we have to deal with water and ice which have different densities and we have to keep the SSA constant for comparison. According to Eq. (1), if the SSA is 30 $m^2 kg^{-1}$, it means that snow is made up of ice spheres of 109 µm radius while a pure water medium will be made of spheres of 100 µm radius. We therefore take this issue into account for both codes. Increasing the LWC in the Mie code will just replace ice spheres by water spheres with a radius lowered according to the ice-water densities ratio. Increasing the LWC in the layered code will decrease the radius of the outer sphere (core + shell), decrease the radius of the core made of ice and increase the thickness of the shell made of water.

For simplicity, we will use the term reflectance as equivalent to albedo, even though the proper term for our calculations and measurements is directional-hemispherical reflectance (Schaepman-Strub et al., 2006). To illustrate model performance and consistency, Fig. 2 presents the reflectance calculated with both codes for pure ice and

TCD
7, 5255–5279, 2013

pure water spheres for a SSA of 30 $m^2 kg^{-1}$. All calculations have been done under direct illumination with a zero zenith angle and for an optically semi-infinite layer. As expected, the minima and maxima are shifted towards shorter wavelengths for water. Both codes show similar results for each medium with an average difference over the 800–1400 nm range lower than 0.4 % and 0.6 % for ice and water respectively.

Figure 3 shows calculations at 1310 nm (wavelength used in subsequent experiments) for snow SSAs of 5 and 30 $m^2 kg^{-1}$ and LWC from 0 to 100 %. At that wavelength ice and water have very close refractive indices, with water absorbing and scattering slightly more. Mie shows reflectance values decreasing with increasing LWC because water absorbs more and because here, when the LWC increases, ice is replaced by water. For the layered code, the reflectance first increases and then decreases as LWC increases. Our understanding is that a small amount of water is creating a thin layer of water around the ice particles. Scattering is then enhanced while the increase in absorption is negligible for low LWC, explaining the increase in reflectance. For higher LWCs, the water shell is thicker and absorption is not negligible anymore so that reflectance decreases. The decrease of reflectance is observed slightly before for smaller SSA because the shell of water is thicker for the same amount of water compared to higher SSA. Average differences between the two codes are of 0.7 and 1.5 % respectively for SSAs of 30 and 5 $m^2 kg^{-1}$ with maximum differences up to 3 %.

However, neither Mie nor the layered codes are representing correctly the location of water in the snowpack for low LWC. Ketcham and Hobbs (1969) showed that in melting snow, water first appears as a meniscus on the ice surface where three grains join. Wet snow therefore obviously has water–ice interfaces, but the water coverage on ice is partial and of variable thickness. For higher LWC, water forms a continuous network (Colbeck, 1973) and even covers all the ice surfaces at sufficiently high LWC, so that the layered code may then be a reasonable approximation of processes, even though the thickness of the water film is never uniform. In any case, we test both codes over a wide LWC range below.

TCD
7, 5255–5279, 2013

4 Results and discussion

The experimental results obtained are summed up in Table 1. Again in this table, the calculated SSAs for wet samples are only apparent values. For four out of the six experiments, both samples from each experiment produced similar data, supporting our claim that our system produces fairly homogeneous snow. However, this does not seen to be valid for both samples with the highest LWC (31 and 32.1 mass %). We propose that these high LWC values lead to percolation, causing large spatial heterogeneities. For both these experiments, the density and LWC may then not correspond well to those of the actual samples whose reflectance were measured, and should only be considered indicative.

Figure 4 compares the reflectances of the wet and frozen samples. The differences are small. The sample cen_8 seems to be an outlier. Figure 5 shows a similar graph for SSA, and compares the SSA of the frozen sample, SSA_{frozen}, to the apparent SSA of the wet sample, SSA_{app}, which we retrieved using the relation from dry snow from Gallet et al. (2009). The presumed outlier of Fig. 4 expectedly also shows up on Fig. 5. The relative difference in reflectance is at the most 3 %, corresponding to a SSA difference of 1 $m^2\,kg^{-1}$, if the outlier is not considered. We also calculated the difference in SSA, SSA_{frozen}–SSA_{app}, and plotted these as a function of LWC in Fig. 6. The correlation between SSA differences and LWC is low with $R^2 = 0.14$ (dashed red line). If the suspected outlier is removed, R^2 values drop to 0.0001 (black solid line). These results show that the difference in SSA is not correlated to the LWC. The mean SSA difference shown in Fig. 6 between frozen and wet samples is 0.5 $m^2\,kg^{-1}$ when the outlier is not considered.

This allows us to propose a simple algorithm to measure the SSA of wet snow in the field. What we measure is the reflectance of wet snow, R_{wet}, from which we deduced an apparent SSA, SSA_{app}, from the relationships f of Gallet et al. (2009):

$$SSA_{app} = f(R_{wet}) \quad (2)$$

TCD
7, 5255–5279, 2013

From Fig. 6, we have determined experimentally that:

$$SSA_{app} = SSA_{frozen} - 0.5\,m^2\,kg^{-1} \quad (3)$$

If we now assume that upon freezing, no structural changes take place except those due to the volume expansion, we then have the actual SSA of the wet snow that verifies:

$$SSA_{wet} = \psi SSA_{frozen}, \quad (4)$$

where ψ is a complex factor that depends on the geometry of the snow and on the distribution of the water in the snow sample. Combining the above 3 equations, we obtain:

$$SSA_{wet} = (f(R_{wet}) + 0.5)\,\psi \quad (5)$$

The general form of ψ can be expressed as a function of the various interfaces in wet and frozen snow. We call $S_{a/i}$ and $S_{a/w}$ the area of the air/ice and air/water interfaces in wet snow and $S_{a/f}$ the area of the interface between the air and the refrozen water in the frozen snow. Equation (4) then becomes:

$$SSA_{wet} = SSA_{frozen} \frac{S_{a/i} + S_{a/w}}{S_{a/i} + S_{a/f}} \quad (6)$$

Because of the expansion upon freezing, $S_{a/w} < S_{a/f}$ and ψ is therefore always less than 1 considering there is no other structural changes. If we make the approximation that wet snow consists of disconnected ice spheres surrounded by a homogenous water layer whose thickness is determined by the LWC, the ice in the wet snow is not in contact with the air so that we then have:

$$SSA_{wet} = SSA_{frozen} \frac{S_{a/w}}{S_{a/f}}. \quad (7)$$

TCD
7, 5255–5279, 2013

Also using Eqs. (4) and (5), we calculate that in this case we have:

$$\mathrm{SSA_{wet}} = (f(R_{\mathrm{wet}}) + 0.5)\left[1 - \mathrm{LWC}\left(1 - \rho_{\mathrm{ice}}/\rho_{\mathrm{water}}\right)\right]^{2/3}. \quad (8)$$

Of course, this expression is only an approximation based on a structural simplification, and we attempt to evaluate it in the subsequent modeling part. Assuming for the moment that this approximation is acceptable, we propose that to measure the SSA of wet snow with DUFISSS, we just need to measure its 1310 nm reflectance, obtain an apparent value from the relationships of Gallet et al. (2009), add 0.5 $\mathrm{m^2\,kg^{-1}}$ to that value, and then multiply by the factor ψ which can be approximately calculated with the coated sphere structural approximation. We note that in general both these additive and multiplicative corrections are small and in opposite directions, so that in most cases corrections are minimal. The error is large only for very small SSAs. For $\mathrm{SSA} \geq 5\,\mathrm{m^2\,kg^{-1}}$, the error is < 10 %, and for $\mathrm{SSA} \geq 10\,\mathrm{m^2\,kg^{-1}}$, the error is < 5 %. Not knowing the LWC results in errors always less than 3 %, for LWC < 0.40.

In practice, omitting these correction often results in errors much smaller than the instrumental error of 10 %, as illustrated in Fig. 7. This suggests that errors caused by the structural approximations used to derive wet snow SSA are most likely very small.

We also estimated the effect of the LWC on the SSA using the Mie and layered codes. For that purpose, we ran both models using the geometry of our DUFISSS instrument as we did in our previous publication (Gallet et al., 2009). This means that the snow is subjected to mostly direct lighting, but also to diffuse light due to the laser diode beam being reflected on the integrating sphere and re-illuminating the sample. We first calculated the reflectance of snow that should be measured by DUFISSS for samples having the properties of our experimental snows. Calculations were performed for dry and for wet snow with the LWCs determined experimentally. Both Mie and layered codes were used. The calculated reflectances were then converted into snow SSA using polynomial fits (Gallet et al., 2009). Slight modifications to the code had to be made, relative to that of Gallet et al. (2009) because of constraints in the layered code, as detailed in the appendix.

TCD
7, 5255–5279, 2013

These calculations yield the apparent SSA of wet snow, as determined in our experiments, and similarly to Fig. 6, we can plot the difference between the SSA of the frozen sample and the apparent SSA of the wet sample. This was done in Fig. 8, where data obtained using both models are plotted together with the experimental data. The outlier identified previously has been omitted. Figure 8 shows that the dry-wet differences are not the same for both codes and for the experimental data. This is expected since neither code actually reproduces the configuration of the actual sample, with respect to liquid water distribution. However, it is interesting to note that both codes show little correlation between the SSA difference and LWC, with correlations of only 0.01 and 0.1. This comforts our experimental result that the SSA difference does not depend on LWC. This also shows that there is no significant contradiction between our experimental data and the layered approximation used to derive Eq. (8), comforting its validity.

5 Conclusions

Gallet et al. (2009) showed that the DUFISSS instrument could measure reliably the SSA of every type of dry snow tested. Here, we show that DUFISSS can also measure the SSA of wet snow. Experimental data and modeling work have shown that the effect of water on the snow reflectance at 1310 nm is weak and depends very little on snow SSA and LWC. Furthermore, in most cases, deriving the SSA of wet snow assuming that its reflectance–SSA relationship is similar to that of dry snow leads to small errors. For an accurate determination of the SSA of wet snow, however, we recommend to correct the SSA value determined using the experimental dry fit of Gallet et al. (2009) by adding $0.5\,m^2\,kg^{-1}$ and multiplying the value obtained by a factor close to 1 that depends on the LWC. Since the correction depends little on the LWC, not knowing the LWC is not critical and assuming a LWC of 10 %, i.e, a corrective factor $\psi = 0.994$ will result in errors < 2 %. Our experimental data ranged from 16 to $38\,m^2\,kg^{-1}$ with LWC from 5 to 32 %. Admittedly, one weakness of this study is that it did not measure snows

TCD
7, 5255–5279, 2013

with very low SSAs. However, given the low or null dependence of the observed effects of water on retrieving snow SSA, we feel that the resulting error caused by extrapolating our conclusion to low SSAs is most likely very small, and in any case smaller than the intrinsic measurement error of the IR reflectance method used, which is 10 % (Gallet et al., 2009).

Appendix A

The calculations done for Fig. 8 follow the DUFISSS configuration detailed in Gallet et al. (2009). Both the Mie and layered codes used calculate the reflectance of a given snow sample which is 25 mm thick. Direct nadir lighting is used and diffuse lighting due to the light reflected by the sample onto the integrating sphere walls is taken into account. A collimation factor of 0.95 for the 1310 nm laser diode is used. The reflectances of both wet and frozen samples are calculated using both codes.

To obtain SSA from reflectance, a polynomial fit is used (Gallet et al., 2009). However, here the polynomial fit had to be recalculated to account for our different calculation conditions. In Gallet et al. (2009), a log-normal distribution of snow grain sizes was used. This could not be used in the layered code because that model splits the sphere that represents the snow particles in a core of ice and a shell of water. The model has a limited range of possibilities for accurate and validated results, meaning that the size and the ratio of the core and the shell are limited and cannot be out of a given range. Using a log-normal distribution generates very large and very small particles that are out of the range accessible to the layered code. We therefore did not use any log-normal distribution in the layered code. To allow meaningful comparisons, we did not use a log-normal distribution in the Mie code either. New polynomial fits were therefore determined for both codes, which are valid for snow grain sizes without a log-normal distribution.

Acknowledgements. FD thanks CEN Grenoble for hosting him to carry out the experimental work. The assistance of François Touvier to operate the snow heater and of Jean-Michel Panel

TCD
7, 5255–5279, 2013

and Jacques Roulle to operate the cold room are gratefully acknowledged. JCG was supported through the project “Long Range transport of Black Carbon and the effect on snow albedo in North East China and in the Arctic” funded by the Norwegian Research Council (Norklima program, project 193717).

References

Aoki, T., Fukabori, M., Hachikubo, A., Tachibana, Y., and Nishio, F.: Effects of snow physical parameters on spectral albedo and bidirectional reflectance of snow surface, J. Geophys. Res.-Atmos., 105, 10219–10236, 2000.

Arnaud, L., Picard, G., Champollion, N., Domine, F., Gallet, J., Lefebvre, E., Fily, M., and Barnola, J. M.: Measurement of vertical profiles of snow specific surface area with a one centimeter resolution using infrared reflectance: Instrument description and validation, J. Glaciol., 57, 17–29, 2011.

Brun, E., Panel, J. M., and Lafeuille, J.: Dielectric measurement of snow liquid water content, in: Fourth International Conference on Atmospheric Icing of Structures Paris, 287–289, 1988.

Colbeck, S.: Theory of Metamorphism of Wet Snow, USACRREL Report 73, United States Army Corps of Engineers, Hanover, NH, 1–11, 1973.

Domine, F., Taillandier, A. S., and Simpson, W. R.: A parameterization of the specific surface area of seasonal snow for field use and for models of snowpack evolution, J. Geophys. Res.-Earth, 112, F02031, doi:10.1029/2006jf000512, 2007.

Domine, F., Gallet, J. C., Barret, M., Houdier, S., Voisin, D., Douglas, T., Blum, J. D., Beine, H., and Anastasio, C.: The specific surface area and chemical composition of diamond dust near Barrow, Alaska, J. Geophys. Res., 116, D00R06, doi:10.1029/2011JD016162, 2011.

Dozier, J. and Painter, T. H.: Multispectral and hyperspectral remote sensing of alpine snow properties, Annu. Rev. Earth Pl. Sc., 32, 465–494, doi:10.1146/annurev.earth.32.101802.120404, 2004.

Flin, F., Brzoska, J. B., Lesaffre, B., Coleou, C. C., and Pieritz, R. A.: Three-dimensional geometric measurements of snow microstructural evolution under isothermal conditions, Ann. Glaciol., 38, 39–44, 2004.

TCD
7, 5255–5279, 2013

Gallet, J.-C., Domine, F., Zender, C. S., and Picard, G.: Measurement of the specific surface area of snow using infrared reflectance in an integrating sphere at 1310 and 1550 nm, The Cryosphere, 3, 167–182, doi:10.5194/tc-3-167-2009, 2009.

Green, R. O., Dozier, J., Roberts, D., and Painter, T.: Spectral snow-reflectance models for grain-size and liquid-water fraction in melting snow for the solar-reflected spectrum, Ann. Glaciol., 34, 71–73, 2002.

Green, R. O., Painter, T. H., Roberts, D. A., and Dozier, J.: Measuring the expressed abundance of the three phases of water with an imaging spectrometer over melting snow, Water Resour. Res., 42, W10402, doi:10.1029/2005wr004509, 2006.

Hall, A.: The role of surface albedo feedback in climate, J. Climate, 17, 1550–1568, 2004.

Ketcham, W. M. and Hobbs, P. V.: An experimental determination of surface energies of ice, Phil. Mag., 19, 1161–1173, doi:10.1080/14786436908228641, 1969.

Legagneux, L., Cabanes, A., and Domine, F.: Measurement of the specific surface area of 176 snow samples using methane adsorption at 77 K, J. Geophys. Res.-Atmos., 107, 4335, NOD17, doi:10.1029/2001jd001016, 2002.

Lemke, P., Ren, J., Alley, R. B., Allison, I., Carrasco, J., Flato, G., Fujii, Y., Kaser, G., Mote, P., Thomas, R. H., and Zhang, T.: Observations changes in snow, ice and frozen ground, in: Climate Change 2007: The Physical Sciences Basis, edited by: Pachauri, R. K. and Reisinger, A., IPCC, Geneva, Switzerland, 338–383, 2007.

Matzl, M. and Schneebeli, M.: Measuring specific surface area of snow by near-infrared photography, J. Glaciol., 52, 558–564, 2006.

Montpetit, B., Royer, A., Langlois, A., Cliche, P., Roy, A., Champollion, N., Picard, G., Domine, F., and Obbard, R.: New shortwave infrared albedo measurements for snow specific surface area retrieval, J. Glaciol., 58, 941–952, doi:10.3189/2012JoG11J248, 2012.

Nolin, A. W. and Dozier, J.: A hyperspectral method for remotely sensing the grain size of snow, Remote Sens. Environ., 74, 207–216, doi:10.1016/s0034-4257(00)00111-5, 2000.

Painter, T. H., Molotch, N. P., Cassidy, M., Flanner, M., and Steffen, K.: Instruments and methods – contact spectroscopy for determination of stratigraphy of snow optical grain size, J. Glaciol., 53, 121–127, 2007.

Picard, G., Arnaud, L., Domine, F., and Fily, M.: Determining snow specific surface area from near-infrared reflectance measurements: numerical study of the influence of grain shape, Cold Reg. Sci. Technol., 56, 10–17, doi:10.1016/j.coldregions.2008.10.001, 2009.

TCD
7, 5255–5279, 2013

Schaepman-Strub, G., Schaepman, M. E., Painter, T. H., Dangel, S., and Martonchik, J. V.: Reflectance quantities in optical remote sensing-definitions and case studies, Remote Sens. Environ., 103, 27–42, doi:10.1016/j.rse.2006.03.002, 2006.
Segelstein, D. J.: The complex refractive index of water, Master's, University of Missouri, Kansas City, 167 pp., 1981.
Stamnes, K., Tsay, S. C., Wiscombe, W., and Jayaweera, K.: Numerically stable algorithm for discrete-ordinate-method radiative-transfer in multiple-scattering and emitting layered media, Appl. Optics, 27, 2502–2509, 1988.
Toon, O. B. and Ackerman, T. P.: Algorithms for the calculation of scattering by stratified spheres, Appl. Optics, 20, 3657–3660, doi:10.1364/ao.20.003657, 1981.
Warren, S. G.: Optical-properties of snow, Rev. Geophys., 20, 67–89, 1982.
Warren, S. G. and Brandt, R. E.: Optical constants of ice from the ultraviolet to the microwave: a revised compilation, J. Geophys. Res.-Atmos., 113, D14220, doi:10.1029/2007jd009744, 2008.
Warren, S. G. and Wiscombe, W. J.: A model for the spectral albedo of snow. 2. Snow containing atmospheric aerosols, J. Atmos. Sci., 37, 2734–2745, 1980.
Wiscombe, W. J. and Warren, S. G.: A model for the spectral albedo of snow. 1. Pure snow, J. Atmos. Sci., 37, 2712–2733, 1980.

TCD
7, 5255–5279, 2013

Table 1. Density, liquid water content (LWC), reflectance at 1310 nm (R in %), and specific surface area (SSA $m^2\,kg^{-1}$) of the samples studied, wet at 0 °C and frozen. SSAs for wet samples are apparent values as defined in text.

Snow sample name	Heat time, min	Density $kg\,m^{-3}$	LWC, mass %	R wet snow	R frozen snow	SSA_{app} wet snow	SSA frozen snow	R frozen – R wet	SSA frozen – SSA_{app} wet
cen_1	45	182	9.6	44.11	44.37	35.5	35.6	0.30	0.10
cen_2	45	182	9.6	43.21	43.26	33.4	33.5	0.05	0.10
cen_3	86	283	31.0	32.15	32.15	18.4	18.4	0.00	0.00
cen_4	86	283	31.0	24.35	25.09	12.1	12.6	0.74	0.50
cen_5	23	208	5.0	43.99	44.39	34.9	35.6	0.40	0.70
cen_6	23	208	5.0	45.03	45.41	36.9	37.7	0.38	0.80
cen_7	90	296	32.1	29.36	30.14	15.9	16.5	0.78	0.60
cen_8	90	296	32.1	43.21	45.70	33.4	38.2	2.49	4.80
cen_9	43	153	7.2	43.01	42.98	33.0	33.0	−0.03	0.00
cen_10	43	153	7.2	44.80	45.12	36.4	37.1	0.32	0.70
cen_11	60	260	21.6	30.82	31.55	17.1	17.8	0.73	0.70
cen_12	60	260	21.6	31.80	32.75	18.0	19.0	0.90	1.00

TCD
7, 5255–5279, 2013

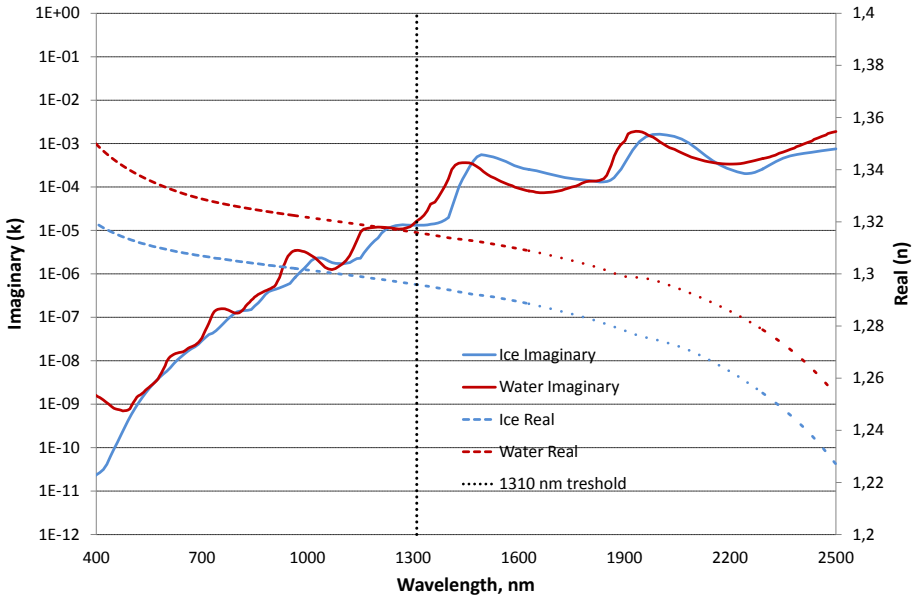

Fig. 1. Real and imaginary indices of refraction of ice (from Warren et al., 2008) and water (from Segelstein, 1981).

TCD
7, 5255–5279, 2013

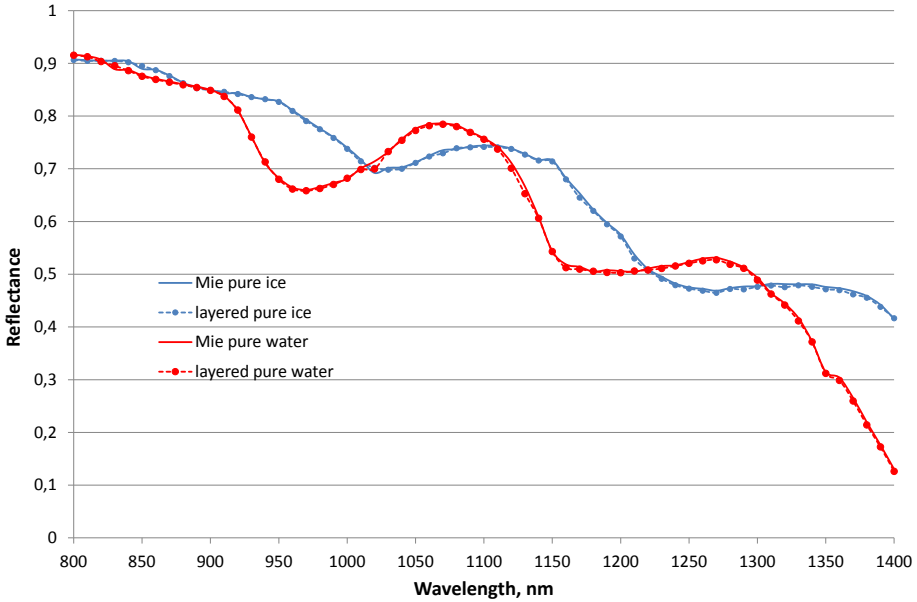

Fig. 2. Reflectance calculated with both codes for snow of SSA=30 $m^2 kg^{-1}$ (pure ice and pure water), density = 300 $kg\,m^{-3}$ and an optically semi-infinite layer.

TCD
7, 5255–5279, 2013

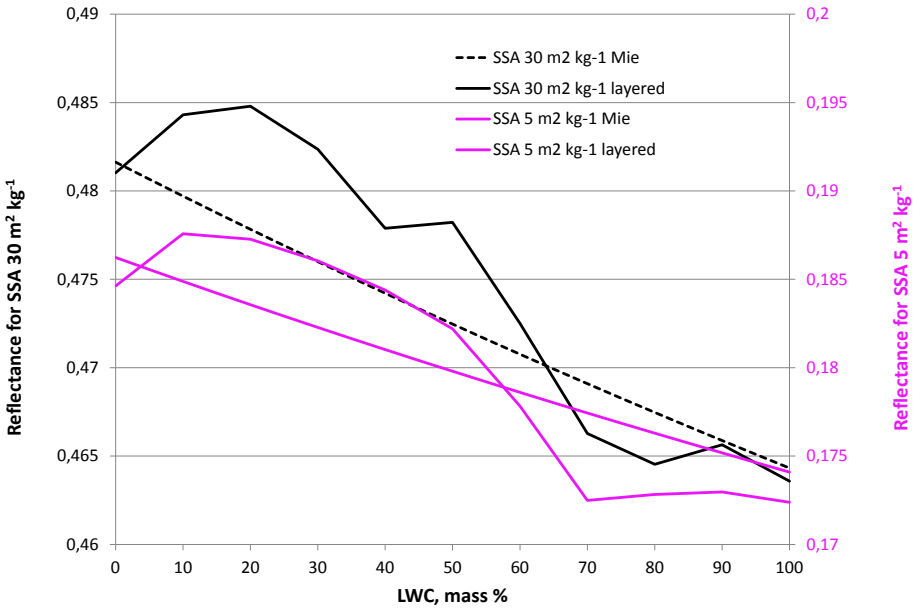

Fig. 3. Effect of the LWC on the reflectance of snow for SSA of 5 and 30 $m^2 kg^{-1}$, density of 300 $kg m^{-3}$ and an optically semi-infinite layer at 1310 nm. Each SSA has its own vertical axis.

TCD
7, 5255–5279, 2013

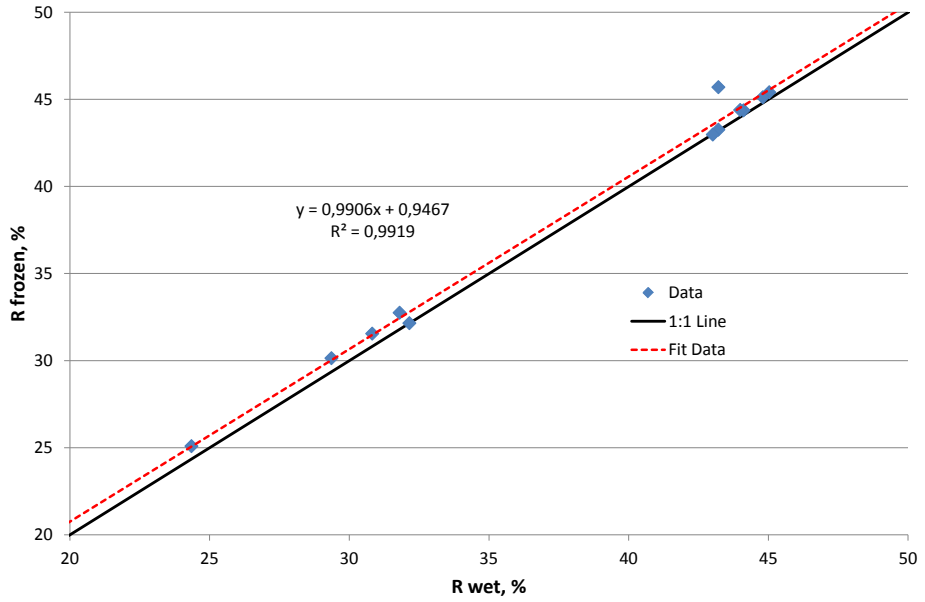

Fig. 4. Correlation between the reflectances of the wet and frozen samples.

TCD
7, 5255–5279, 2013

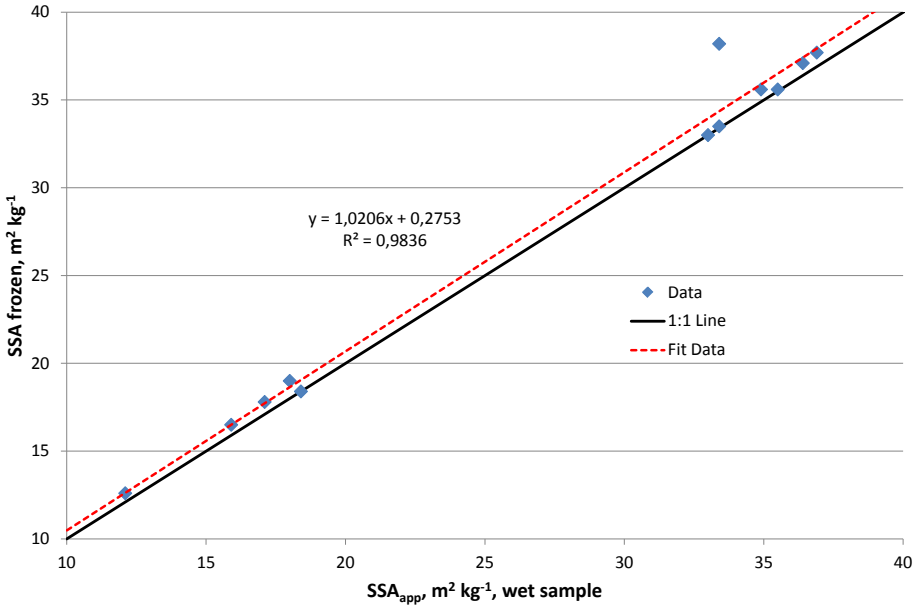

Fig. 5. Correlation between the SSAs of the frozen samples, SSA_{frozen}, and the apparent SSA of the wet samples, SSA_{app}. SSA_{app} was determined from reflectance using the algorithm developed for dry snow.

TCD
7, 5255–5279, 2013

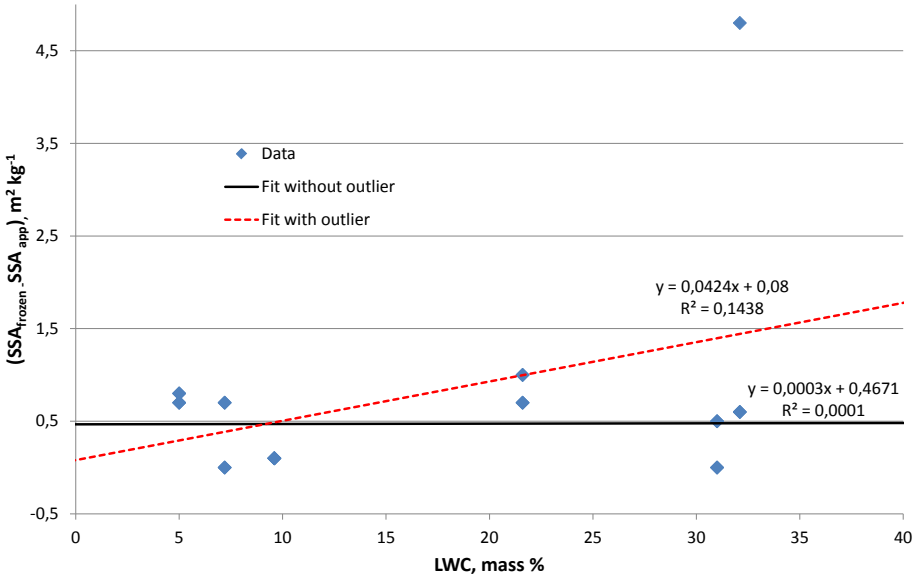

Fig. 6. Difference between the SSA of the frozen sample and the apparent SSA of the wet sample (SSA_{frozen}–SSA_{app}) as a function of LWC.

TCD
7, 5255–5279, 2013

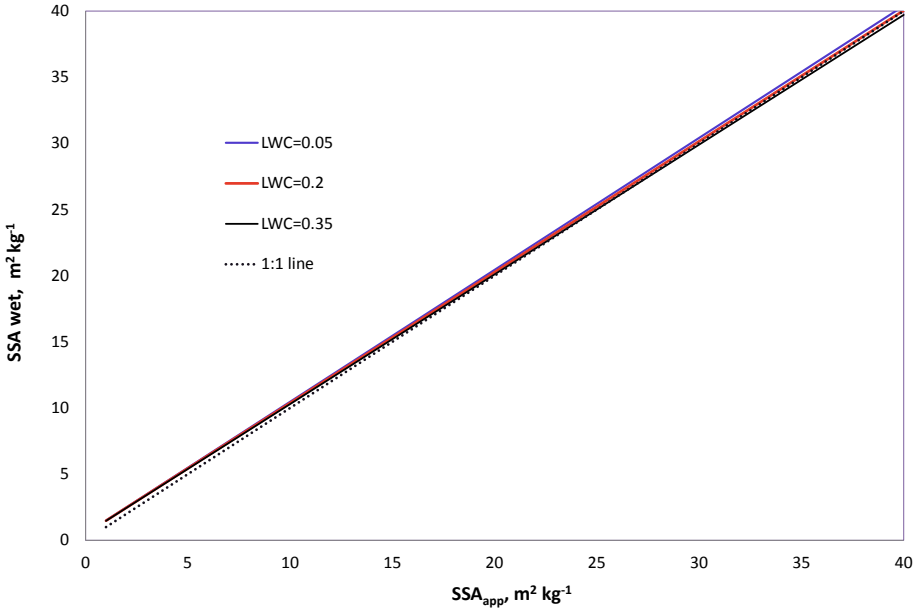

Fig. 7. Relationship between the apparent SSA of a wet snow sample determined with DU-FISSS using dry fit and that of the same sample whose SSA has been corrected according to Eq. (8) that take into account reflectance and expansion effects. Calculations have been done for two realistic LWC of snow.

TCD
7, 5255–5279, 2013

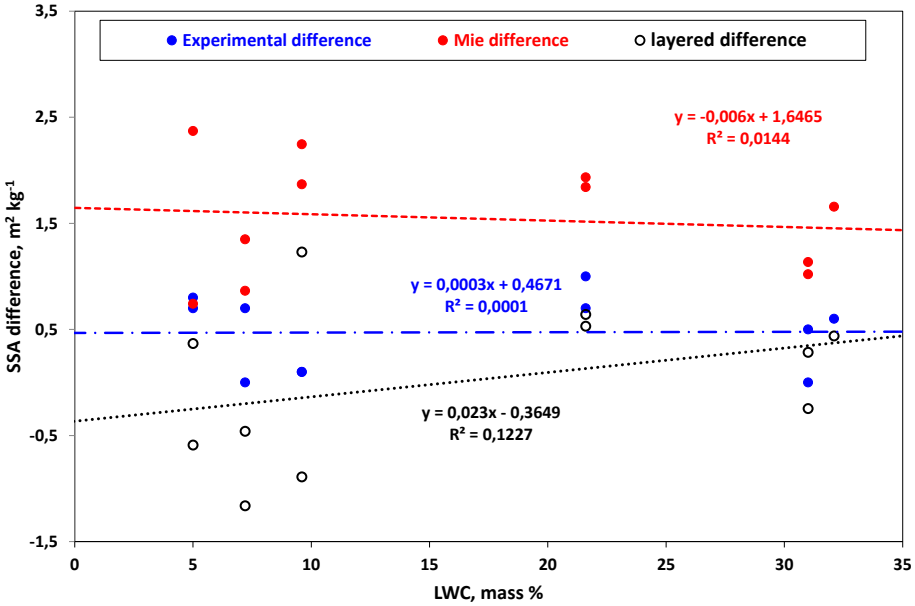

Fig. 8. SSA differences between frozen and wet samples from measurements (blue) and estimated with models calculations with Mie (red) and the layered code (black).

TCD
7, 5255–5279, 2013